Field dependence of the zero energy density of states around vortices in an anisotropic gap superconductor

N. Nakai,[1,*] P. Miranović,[2] M. Ichioka,[3] and K. Machida[3]

[1] *Yukawa Institute for Theoretical Physics, Kyoto University, Kyoto 606-8502, Japan*
[2] *Department of Physics, University of Montenegro, Podgorica 81000, Serbia and Montenegro*
[3] *Department of Physics, Okayama University, Okayama 700-8530, Japan*

(Dated: February 2, 2008)

It is shown theoretically that the Sommerfeld coefficient $\gamma(B)$ in the mixed state contains useful information on the gap topology in a superconductor. We accurately evaluate $\gamma(B)$ against magnetic induction B by using microscopic quasi-classical theory. The linear portion in $\gamma(\propto B)$ relative to B_{c2} and its slope in low field faithfully corresponds to the gap anisotropy, so that we can distinguish the nodal gap and the anisotropic full gap, and estimate the magnitude of the gap anisotropy.

PACS numbers: 74.25.Op, 74.25.Qt, 74.25.Jb, 74.70.Ad

There has been much attention focused on exotic superconductors in recent years, because various new types of superconductors are successfully synthesized. For example, high T_c cuprates and $CeCoIn_5$ are thought that the superconducting state with d-wave pairing is realized. In the case of UPt_3 [1] and Sr_2RuO_4 [2], the superconducting state is thought to be a spin triplet pairing state. Only for a few superconductors, however, the realized pairing function has been conclusively determined as for the gap structure and its parity. Needless to say, it is crucial to know these when we understand its pairing mechanism.

One of the standard methods to resolve the gap structure is to use the temperature (T) dependence of physical quantities, such as the specific heat $C(T)$, the thermal conductivity $\kappa(T)$ and the spin lattice relaxation time $T_1^{-1}(T)$. These comprise a unique set of characteristic T-dependences, allowing us to extract the gap topology; In the case of the nodal gap, where the gap in momentum space is zero along a line on the Fermi surface, $C(T) \propto T^2$, $\kappa(T) \propto T^2$ and $T_1^{-1}(T) \propto T^3$ [3]. In contrast, these are all activation type for full gap case. It is often the case that these T-dependences are masked by other contributions such as impurities, phonon, nuclear spin, etc. Thus it is difficult to definitely conclude the gap anisotropy by the T-dependence of these quantities alone. We certainly need another methods to supplement this situation on top of existing ones.

The magnetic field (B) in a superconductor adds a new dimension: The specific heat and thermal conductivity measurements in the mixed state as a function of B give rise to additional information on low-lying excitation spectrum induced around vortices, which sensitively reflects the gap structure [4, 5]. In fact it has been already demonstrated that the orientational Sommerfeld coefficient $\gamma(\theta)$ and thermal conductivity $\kappa(\theta)$ show a characteristic oscillation with the relative angle θ between the field direction and the direction of the gap node (or minimum) [6, 7, 8, 9, 10, 11, 12]. This allows us to precisely determine the gap anisotropy.

As for observation of low-lying quasi-particle excitations in the mixed state, scanning tunneling microscopy (STM) provides a direct way to probe the spatial extension of these quasi-particles [13]. STM experiments on $2H$-$NbSe_2$ comprise rich information on the gap structure of this system [14]. However in this method, as well as angle-resolved photoemission spectroscopy (ARPES) which yields momentum space information [15, 16, 17], observable materials are restricted due to the surface-sensitivity.

Thus it is quite desirable to establish another method to probe the gap structure through bulk measurements. Here we propose the field-dependence of specific heat measurement at low temperature, namely the Sommerfeld coefficient $\gamma(B)$ in the mixed state. We demonstrate that the precise $\gamma(B)$ measurement at low field yields an important piece of information on the degree of the gap anisotropy, or the ratio of the minimum gap and maximum gap in a superconductor.

This type of experiments has been done in the past on a variety materials such as Nb [18], $2H$-$NbSe_2$ [19, 20], $CeRu_2$ [21], $LuNi_2B_2C$ [22], $YBa_2Cu_3O_7$ [23], Sr_2RuO_4 [12] and $Pr_{2-x}Ce_xCuO_{4-\delta}$ [24]. However, because of lack of theoretical detailed calculations, these data remain largely to be analyzed. Theoretically $\gamma(B)$ was interpreted in terms of "rigid normal core concept" [25], that is, $\gamma(B) \propto B/B_{c2}$ for superconductors with full gap because each flux carries a certain zero-energy density of states (ZDOS). Volovik succeeded in describing *qualitatively* $\gamma(B)$ ($\propto \sqrt{B}$) for the nodal gap superconductor [26]. However, there are many experimental data that $\gamma(B)$ shows convex curve, including $\sqrt{B}$-like behavior, even in full-gap superconductors. So far no one has studied this problem in a *quantitative* level which allows us to examine abundant experimental data $\gamma(B)$ in order to deduce the anisotropy of the gap structure, or the ratio of the minimum and maximum gaps, including the nodal case where the minimum gap is zero.

The quasi-classical Eilenberger framework [27] is most suited for the present purpose, which is microscopic valid

for almost all superconductors where $k_F\xi \gg 1$. We assume a superconductor in the clean limit and with the cylindrical Fermi surface, which does not alter our main conclusion essentially valid for three-dimensional case too.

We introduce the pair potential $\Delta(\mathbf{r},\theta)$, the vector potential $\mathbf{A}(\mathbf{r})$ and the quasi-classical Green's functions $g(\mathrm{i}\omega_n,\mathbf{r},\theta)$, $f(\mathrm{i}\omega_n,\mathbf{r},\theta,)$ and $f^\dagger(\mathrm{i}\omega_n,\mathbf{r},\theta)$, where $\mathbf{r}$ is the center of mass coordinate of the Cooper pair. The direction of the relative momentum of the Cooper pair, $\hat{\mathbf{k}} = \mathbf{k}/|\mathbf{k}|$; $\hat{\mathbf{k}} = (\cos\theta, \sin\theta)$, is denoted by the polar angle θ relative to $\mathbf{x}$-direction. The Eilenberger equation is given by

$$\left\{\omega_n + \frac{\mathrm{i}}{2}\mathbf{v}_\mathrm{F}\cdot\left(\frac{\nabla}{\mathrm{i}} + \frac{2\pi}{\phi_0}\mathbf{A}(\mathbf{r})\right)\right\} f(\mathrm{i}\omega_n,\mathbf{r},\theta) = \Delta(\mathbf{r},\theta)g(\mathrm{i}\omega_n,\mathbf{r},\theta), \quad (1)$$

$$\left\{\omega_n - \frac{\mathrm{i}}{2}\mathbf{v}_\mathrm{F}\cdot\left(\frac{\nabla}{\mathrm{i}} - \frac{2\pi}{\phi_0}\mathbf{A}(\mathbf{r})\right)\right\} f^\dagger(\mathrm{i}\omega_n,\mathbf{r},\theta) = \Delta^*(\mathbf{r},\theta)g(\mathrm{i}\omega_n,\mathbf{r},\theta), \quad (2)$$

$$g(\mathrm{i}\omega_n,\mathbf{r},\theta) = [1 - f^\dagger(\mathrm{i}\omega_n,\mathbf{r},\theta)f(\mathrm{i}\omega_n,\mathbf{r},\theta)]^{\frac{1}{2}}, \quad (3)$$

where $\mathrm{Re}\, g(\mathrm{i}\omega_n,\mathbf{r},\theta) > 0$ and $\mathbf{v}_\mathrm{F} = v_\mathrm{F}\hat{\mathbf{k}}$ is the Fermi velocity. ϕ_0 is flux quantum.

The external field $\mathbf{H}$ is applied along $\mathbf{z}$-direction. With the symmetric gauge, the vector potential is written as $\mathbf{A}(\mathbf{r}) = (1/2)\mathbf{H}\times\mathbf{r} + \mathbf{a}(\mathbf{r})$. Here $\mathbf{a}(\mathbf{r})$ is related to the internal field $\mathbf{h}(\mathbf{r})$, where $\mathbf{h}(\mathbf{r}) = \nabla\times\mathbf{a}(\mathbf{r})$. The pairing interaction is assumed separable $V(\theta,\theta') = V_0\phi(\theta)\phi(\theta')$ so that the pair potential is $\Delta(\mathbf{r},\theta) = \Delta(\mathbf{r})\phi(\theta)$.

We numerically [4, 5, 8] solve Eqs. (1)-(3) with the self-consistent conditions for $\Delta(\mathbf{r},\theta)$ and $\mathbf{a}(\mathbf{r})$;

$$\Delta(\mathbf{r}) = N_0V_0 2\pi T\sum_{\omega_n>0}^{\omega_c}\int_0^{2\pi}\frac{d\theta'}{2\pi}\phi(\theta')f(\mathrm{i}\omega_n,\mathbf{r},\theta'), \quad (4)$$

$$\mathbf{j}(\mathbf{r}) = -\frac{\pi\phi_0}{\kappa^2\Delta_0\xi^3}2\pi T\sum_{\omega_n>0}^{\omega_c}\int_0^{2\pi}\frac{d\theta}{2\pi}\frac{\hat{\mathbf{k}}}{\mathrm{i}}g(\mathrm{i}\omega_n,\mathbf{r},\theta), \quad (5)$$

where $\mathbf{j}(\mathbf{r}) = \nabla\times\nabla\times\mathbf{a}(\mathbf{r})$, N_0 is the density of states at the Fermi energy in the normal state. The cut-off energy is set as $\omega_\mathrm{c} = 20T_\mathrm{c}$. $\kappa = \sqrt{7\zeta(3)/72}(\Delta_0/T_\mathrm{c})\kappa_\mathrm{GL}$. $\zeta(3)$ is Riemann's zeta function. The Ginzburg-Landau parameter is set as $\kappa_\mathrm{GL} = 9.0$. Δ_0 is the uniform gap at $T = 0$.

The local DOS of the energy E is given by

$$N(E,\mathbf{r}) = N_0\int_0^{2\pi}\frac{d\theta}{2\pi}\mathrm{Re}\, g(\mathrm{i}\omega_n\to E+\mathrm{i}\eta,\mathbf{r},\theta), \quad (6)$$

where g is calculated by the above Eilenberger equations with $\mathrm{i}\omega_n\to E+\mathrm{i}\eta$, using the solution Δ and $A(\mathbf{r})$ by the self-consistent calculation. We typically use $\eta = 0.01\Delta_0$.

The calculation for Green's functions is performed at $T/T_\mathrm{c} = 0.1$ within the vortex lattice unit cell, which is divided into 81×81 mesh points. In this study, we assume that vortices form a triangular lattice. One of the nearest neighbor vortices is situated along $\mathbf{x}$-direction.

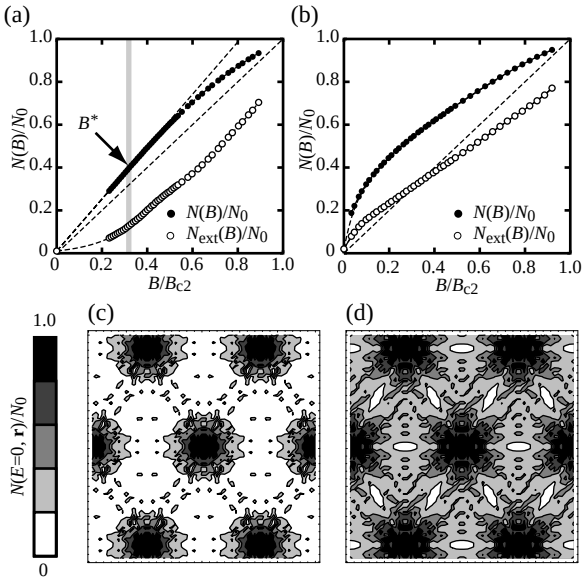

FIG. 1: (a) and (b) show field dependences of ZDOS. The filled (open) circles are for the total (extend) ZDOS. In (c) and (d) density maps of ZDOS are shown around a vortex core at the center and neighbor vortex cores. $B/B_{c2} = 0.24$. The density height of the vortex center is truncated by 1. Isotropic gap case ((a) and (c)) and line-node gap case ((b) and (d)) are presented.

The gap function is taken as $\phi(\theta) = 1$ for the isotropic gap case, and $|\phi(\theta)| = \sqrt{1-\cos 6\theta} = \sqrt{2}\,|\cos 3\theta|$ for the line-node gap case. The gap function with finite minimum gap is chosen as $\phi(\theta) = (1-\alpha\cos 6\theta)/\sqrt{1+\alpha^2/2}$, where α denotes the degree of the gap anisotropy, whose sign and magnitude characterize the gap structure. Here hexagonal crystal symmetry is assumed.

The total ZDOS or $N(B)$ is the spatial average of $N(E=0,\mathbf{r})$, which is given by $N(B) = \int N(E=0,\mathbf{r})d\mathbf{r}/\int d\mathbf{r}$. This is related to $\gamma(B)$ at $T\to 0$ limit. To characterize delocalized contribution to total ZDOS, we define "extended ZDOS" by $N_\mathrm{ext}(B) = \int_c N(E=0,\mathbf{l})d\mathbf{l}/\int_c d\mathbf{l}$, where the path of the integration $\int_c\cdots d\mathbf{l}$ is along the boundary of the Wigner-Seitz cell. Thus $N_\mathrm{ext}(B)$ is a useful quantity, related to the states outside of the vortex core. This is directly measurable by STM, and would somehow be related to the thermal conductivity.

Let us now show our results deduced from extensive self-consistent calculations. We first take up two extreme cases for the isotropic gap and line node gap: In Fig. 1 (a), the field dependence of the ZDOS for the isotropic gap is shown. It is seen that $N(B)$ is linear for smaller induction field B up to a certain field B^*. Beyond B^* $N(B)$ becomes curving up to the upper crit-

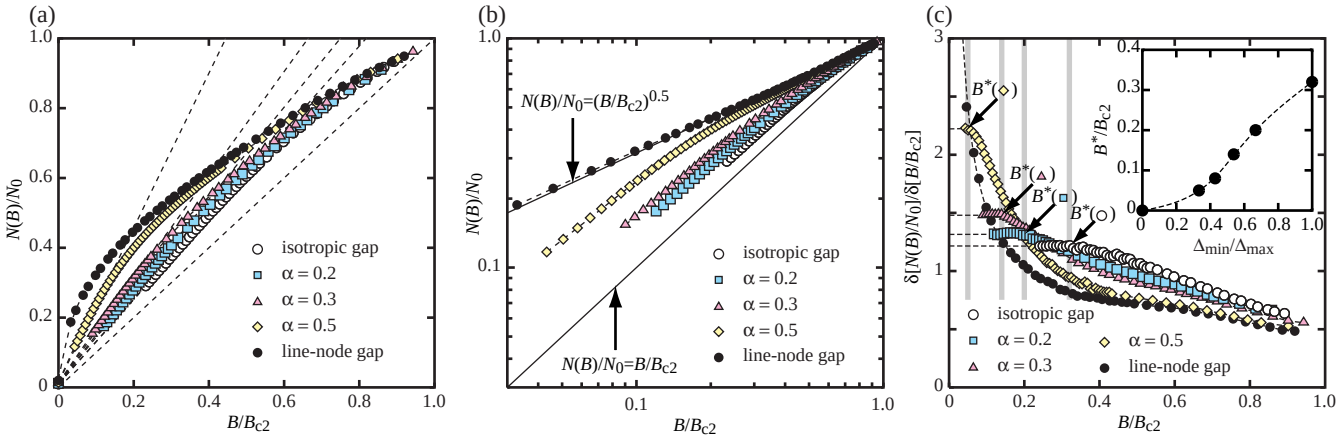

FIG. 2: (color) (a) Field dependence of $N(B)$ for anisotropic gap cases. Plotted data are for $\alpha = 0, 0.2, 0.3, 0.5$ and the line-node from bottom to top. (b) The same data are replotted in logarithmic scale. (c) Field dependence of derivative $\delta N(B)/\delta B$, i.e., slope of $N(B)$. From right to left shadow lines indicate each B^* for $\alpha = 0, 0.2, 0.3, 0.5$. In the inset, B^*/B_{c2} is plotted as a function of $\Delta_{\rm min}/\Delta_{\rm max}$. $\Delta_{\rm min} = \phi(\theta = 0)$ ($\Delta_{\rm max} = \phi(\theta = \pi/6)$) is the minimum (maximum) of the gap function $\phi(\theta)$.

ical field B_{c2}. As for the extended ZDOS $N_{\rm ext}(B)$, it is concaved all the way up to B_{c2}.

The presence of B^* can be understood as follows: As B increases, considerable overlapping of ZDOS at each core makes the linear behavior in $N(B)$ change to non-linear at B^*. Up to B^*, vortices carry independently a certain ZDOS to add up. We see it from Fig. 1 (c) that ZDOS is quite small in a large part of unit cell except for the small core region. This is compared with that for line node case in Fig. 1 (d). It is emphasized that the low field linear behavior in $N(B)$ superficially accords with the so-called rigid normal core model [25], but the situation is more interesting and subtle: (1) There exists a crossover field B^* from linear to non-linear even in the isotropic gap case, which is a key fact important in the anisotropic case below. (2) Even in small B region $N_{\rm ext}(B)$ is substantial, meaning that vortex cores are overlapped there. This invalidates rigid normal core picture [25].

The line node gap case as an extreme anisotropic one is shown in Figs. 1 (b) and (d). Both curves of $N(B)$ and $N_{\rm ext}(B)$ are convex with no linear part at low B. These results are totally different from those of the isotropic case. In particular, the small field behavior is affected by the presence of nodes. In the nodal gap case $N_{\rm ext}(B)$ increases rapidly with B as seen from Fig. 1 (b), because the quasi-particle wave functions with zero-energy extend to far outside of the vortex core due to the node (see Fig. 1 (d)). Therefore $N_{\rm ext}(B)$ shows the convex behavior at lowest B, which is contrasted with the concave behavior of $N_{\rm ext}(B)$ at small B in Fig. 1 (a). Moreover $N(B)$ is non-linear from the lowest field because the quasiparticles near the gap node are free from confinement in the core region, as clearly seen in Figs. 1 (b) and (d).

These results again seem to coincide superficially with Volovik's Doppler shift calculation [26]. Here we emphasize that Volovik calculation neglects the core contribution coming from the localized quasi-particles, taking into account the extended quasi-particle contribution. Volovik result ($N(B) \propto \sqrt{B}$) is, strictly speaking, only valid for smallest B region and is qualitative in nature.

We now come to our main results for general anisotropic gap case; In Figs. 2 (a) and (b), we display $N(B)$ for various values of α, including the above extreme cases with line node. It is seen from these that (A) For $\alpha \neq 1$ $N(B)$ is linear in B at lower fields. (B) The linear B region becomes limited to lower B as α increases. This can be easily seen in logarithmic plot of Fig. 2 (b), where the slopes ($\alpha \neq 1$) in logarithmic plot change from $N(B)/N_0 \propto B/B_{c2}$ to $(B/B_{c2})^{0.5}$ as B increases. There exists always a crossover field B^* for general α, whose precise value is determined below. (C) At higher field near B_{c2}, $N(B)$ behaves similarly, independent of α values. It is clear that $N(B)$ is not described by a single exponential form $N(B) \propto B^p$ covering all B region except for the nodal gap case. Near B_{c2} the exponent p is approximated to be 0.5 for all curves.

These results are interpreted along the same line above, namely, in terms of quasi-particle's localized-delocalized crossover upon varying B. In the region $B < B^*$ each vortex core independently contributes to the DOS at zero energy while $B > B^*$ the quasi-particles are brought with flux lines overlapping each other, making $N(B)$ non-linear. Thus a question is how B^* is correlated to the gap anisotropy α.

We exhibit the derivative $\delta N(B)/\delta B$ in Fig. 2 (c). If $N(B)$ is linear in B, the derivative is a constant and equals to the slope of $N(B)$ near $B = 0$. This linear slope constant, indicating how much DOS is brought into a system by a flux line, increases with α. This implies that

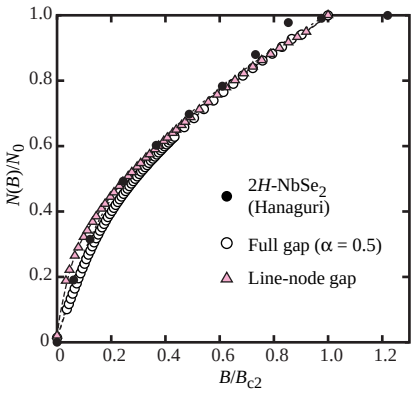

FIG. 3: (color) Comparison with the $\gamma(B)$ in $2H$-$NbSe_2$ [19] with our results for $\alpha = 0.5$ and line node gap.

the ZDOS per vortex increases with the gap anisotropy. Physically it is because the average core radius measured by the extension of ZDOS around a core is effectively larger for larger gap anisotropy.

It is clearly seen from Fig. 2 (c) that there is a constant $\delta N(B)/\delta B$ region up tp B^* for each value of α. As shown in the inset of Fig. 2 (c), this crossover field B^* progressively decreases as the ratio of the minimum and maximum gaps grows, or α increases towards 1. In the nodal gap case, the derivative $\delta N(B)/\delta B$ is diverging because the exponent p in $N(B)$ is less than unity [28]. Thus it is possible to estimate the degree of the gap anisotropy α by identifying B^* through specific heat measurement.

For illustrative purpose, we show the comparison between the $\gamma(B)$ data of $2H$-$NbSe_2$ [19] and our results ($\alpha = 0.5$ and line node case) in Fig. 3. $2H$-$NbSe_2$ is a anisotropic but full gap superconductor. While it is possible even to say that $\gamma(B) \propto \sqrt{B}$ at high fields, $\gamma(B)$ deviates from $\sqrt{B}$-behavior at low fields. The low field data fit to $\alpha = 0.5$ rather than line node gap. The anisotropy $\alpha = 0.5$ is also estimated by the recent ARPES data [17] and also by our previous identification [29].

In order to identify the α value in the actual measurement, we must examine the applicability of the present approach. The possible obstacles, which are not considered here are following: (1) Non-magnetic impurities certainly modify $N(B)$ behavior as discussed elsewhere [30, 31]. One needs samples in clean limit. (2) The actual superconductors are often multi-band system, or multi-gap one. Typical example is MgB_2 where distinct two different gaps are assigned for two-bands. In fact $N(B)$ consists of two linear lines [32], each segment is explained in terms of isotropic gap [33, 34]. Thus it is possible to separate out the multi-gap effect. Such multi-gap behavior is seen in various systems, e.g. Sr_2RuO_4 [12], $2H$-$NbSe_2$ [20] or $CeRu_2$ [21] etc. For $2H$-$NbSe_2$, other measurements [16, 17] imply multi gaps. (3) Since there exists the Fermi velocity anisotropy, one may concern its effect on the present conclusion. It turns out that it does not alter our conclusion essentially [35]. (4) Although we considered here 2D system, 3D effect also is checked. We find that it does not also change our conclusion because $N(B)$ is a bulk quantity. Thus we believe that a careful $N(B)$ measurement at low enough T is a powerful method to identify the gap anisotropy.

We are grateful to Y. Matsuda, T. Sakakibara, K. Izawa, T. Hanaguri, T. Kiss and J. E. Sonier for useful discussions. One of the authors (N. N.) is supported by a Grant-in-Aid for the 21st Century COE "Center for Diversity and University in Physics".

* nakai@yukawa.kyoto-u.ac.jp

[1] K. Machida et al., J. Phys. Soc. Jpn., **58**, 4116 (1989); ibid, **68**, 3364 (1999).
[2] For a review, see A. P. Mackenzie and Y. Maeno Rev. Mod. Phys. **75**, 657 (2003).
[3] For example, see M. Sigrist and K. Ueda, Rev. Mod. Phys. **63**, 239 (1991).
[4] M. Ichioka *et al.*, Phys. Rev. B **55**, 6565 (1997).
[5] M. Ichioka *et al.*, Phys. Rev. B **59**, 184 (1999); ibid, **59**, 8902 (1999).
[6] I. Vekhter *et al.*, Phys. Rev. B **59** 9023 (1999).
[7] K. Maki *et al*, Phys. Rev. B **65**, 140502 (2002).
[8] P. Miranović *et al.*, Phys. Rev. B **68**, 052501 (2003).
[9] K. Izawa *et al.*, Phys. Rev. Lett. **89**, 137006 (2002).
[10] T. Park *et al.*, Phys. Rev. Lett. **90**, 177001 (2003).
[11] H. Aoki *et al.*, J. Phys. Condens. Matter **16**, L13 (2004).
[12] K. Deguchi *et al.*, Phys. Rev. Lett. **92**, 047002 (2004).
[13] H. Sakata *et al.*, Phys. Rev. Lett. **84**, 1583 (2000).
[14] H. F. Hess *et al.*, Phys. Rev. Lett. **64**, 2711 (1990).
[15] A. Damascelli *et al.*, Rev. Mod. Phys. **75**, 473 (2003).
[16] T. Yokoya *et al.*, Science **294**, 2518 (2001) .
[17] T. Kiss, thesis (The University of Tokyo, 2004).
[18] J. Ferreira da Silva *et al.*, Physica **41**, 409 (1969).
[19] T. Hanaguri *et al.*, Physica B **329-333**, 1355 (2003).
[20] E. Boaknin *et al.*, Phys. Rev. Lett. **90**, 117003 (2003).
[21] M. Hedo *et al.*, J. Phys. Soc. Jpn. **67**, 272 (1998).
[22] M. Nohara *et al.*, J. Phys. Soc. Jpn. **66**, 1888 (1997).
[23] Y. Wang *et al.,* Phys. Rev. B **63**, 094508 (2001).
[24] H. Balci and R. L. Greene, cond-mat/0402263.
[25] See for this concept, P. G. de Gennes, *Superconductivity of Metals and Alloys* (W.A. Benjamin, New York, 1966).
[26] G. E. Volovik, JETP Lett. **58**, 469 (1993).
[27] G. Eilenberger, Z. Phys. **214**, 195 (1968).
[28] The present "linear" line node gives $p \sim 0.5$ while the "quadratic" node does $p \sim 0.25$. Thus we can determine the power behavior of the gap function around the node.
[29] N. Hayashi *et al.*, Phys. Rev. Lett. **77**, 4074 (1996).
[30] P. Miranovic *et al.*, cond-mat/0312420.
[31] T. Kita, cond-mat/0311562.
[32] F. Bouquet *et al.*, Phys. Rev. Lett. **89**, 257001 (2002).
[33] N. Nakai *et al.*, J. Phys. Soc. Jpn. **71**, 23 (2002).
[34] M. Ichioka *et al.*, preprint.
[35] N. Nakai, private communication.